9

Wood Growth/Morphology

Dušica Janošević, Katarina Vojisavljević, Ilinka Pećinar, Dragana Bartolić and Aleksandra Lj. Mitrović*

Cell wall structure of tensile flexure wood fibers in *Populus x euramericana*

https://doi.org/10.1515/hf-2025-0052 Received April 25, 2025; accepted July 4, 2025; published online July 22, 2025

Abstract: In response to gravitropic environmental stimuli, woody angiosperms develop tension wood (TW). Typical TW fibers are characterized by an inner gelatinous cell wall (c.w.) layer (G-layer). On the other hand, in response to mechanical stimuli, woody plants develop flexure wood. Flexure wood formed under tension in angiosperms is termed tensile flexure wood (TFW). Similarly to TW, TFW represents an increased source of non-recalcitrant cellulose for biofuel production. Histochemical, SEM, and Raman microspectroscopic analyses of TFW of juvenile Populus x euramericana formed in response to severe long-term static bending were performed. The presence of lignin in the G-layer, higher syringyl/guaiacyl ratio, and differences in lignin structure in TFW compared to normal wood, revealed by histochemical analysis, was confirmed by Raman microspectroscopy. Additionally, Raman microspectroscopy indicated differences in cellulose and hemicellulose structure and pectin methylesterification. The G-layer and compound middle lamella contribute to the response to bending by opposite shifts of the orientation-sensitive cellulose band

oand
In response t
and branche

*Corresponding author: Aleksandra Lj. Mitrović, Institute for Multidisciplinary Research, University of Belgrade, Kneza Višeslava 1, 11030 Belgrade, Serbia; and Center of Excellence for Green Technologies, Institute for Multidisciplinary Research, University of Belgrade, Kneza Višeslava 1, 11030 Belgrade, Serbia, E-mail: mita@imsi.rs. https://orcid.org/0000-0003-4211-3575

Dušica Janošević, Faculty of Biology, University of Belgrade, Studentski trg 16, 11158 Belgrade, Serbia, E-mail: dusjan@bio.bg.ac.rs. https://orcid.org/ 0000-0002-3541-4153

Katarina Vojisavljević, Institute for Multidisciplinary Research, University of Belgrade, Kneza Višeslava 1, 11030 Belgrade, Serbia,

E-mail: kvojisavljevic@imsi.rs. https://orcid.org/0000-0002-5318-2309

Ilinka Pećinar, Faculty of Agriculture, University of Belgrade, Nemanjina 6, 11080 Beograd, Serbia, E-mail: ilinka@agrif.bg.ac.rs. https://orcid.org/0000-0002-5332-4696

Dragana Bartolić, Institute for Multidisciplinary Research, University of Belgrade, Kneza Višeslava 1, 11030 Belgrade, Serbia; and Center of Excellence for Green Technologies, Institute for Multidisciplinary Research, University of Belgrade, Kneza Višeslava 1, 11030 Belgrade, Serbia, E-mail: dragana.bartolic@imsi.rs. https://orcid.org/0000-0002-9337-9288

attributed to the glycosidic C–O–C bond. SEM micrographs revealed the c.w. ultrastructure of TFW fibers. The presented findings encourage further investigation of TFW in terms of both changes in c.w. structure as a mechanical acclimation to stem bending and its potential for biofuel production.

Keywords: cell wall; gelatinous fibers; *Populus x euramericana* cl. NS 11-8; tensile flexure wood

Abbreviations

c.w. cell wall

CML compound middle lamella

GL gelatinous layer
NW normal wood
SCW secondary cell wall
SL S₂ layer of SCW in NW
TFW tensile flexure wood

1 Introduction

In response to gravitropic environmental stimuli in stems and branches, woody plants develop a reaction wood to overcome stem lean (Scurfield 1973; Timell 1969). Reaction wood in angiosperms is called tension wood (TW). TW contains more cellulose and less lignin. TW fibers, gelatinous fibers (G-fibers), differ anatomically from normal wood (NW) fibers formed in the absence of stimuli or from opposite wood (OW) fibers located opposite to the TW in the same growth ring. Typical G-fibers are characterized by an inner gelatinous cell wall (c.w.) layer (G-layer). The G-layer may be formed inside the S3 layer or replace the S3 layer and a part or the whole S2 layer (Abedini et al. 2015; Dadswell and Wardrop 1955). On the other hand, in response to mechanical stimuli (such as wind or artificial bending treatments), woody plants develop "flexure wood" (Telewski 1989), which shows some differences compared to reaction wood. Recently, for "flexure wood" formed under tension in angiosperms, the term "tensile flexure wood" (TFW) was proposed (Roignant et al. 2018).

Compared to TW fibers, TFW fibers show a thinner G-layer (with a higher microfibrillar angle) and a thinner S-layer (Niez et al. 2020; Roignant et al. 2018). Similarly to TW (Donaldson and Singh 2016), TFW represents an increased source of non-recalcitrant cellulose for biofuel production (Urbancsok et al. 2023).

Further studies of wood c.w. differentiation as a response to bending were suggested (Roignant et al. 2018). There is no data on the alterations in the structure/composition of c.w. polymers in TFW fibers. Histochemical, SEM, and Raman microspectroscopic analysis of TFW fibers in juvenile *Populus x euramericana* cl. NS 11-8 trees formed in response to severe long-term static bending were performed and discussed regarding both changes in c.w. structure as a mechanical acclimation to stem bending and its potential for biofuel production.

2 Materials and methods

2.1 Plant material and sample collection

Populus x euramericana cl. NS 11-8 juvenile trees, were grown from 20 cm long cuttings, a gift from the Institute of Lowland Forestry and Environment (ILFE), University of Novi Sad. The cuttings were grown in plastic pots $20 \times 20 \times 20$ cm from March 2011 to April 2012 (shoots were about 1.2 m high), outdoors in Belgrade, Serbia (44 49N, 20 29E). Bending was applied by wiring from April to October 2012 (the bending angle was about 90°, Prokopijević et al. 2022). Control plants of the same age were grown under the same conditions as the bent plants but without the bending treatment. Stem samples at stem base from both control and bent trees were collected in October 2012.

2.2 Histochemical analysis

For histochemical analysis unfixed, untreated, dried stem cross-sections, 70 µm thick, of control and bent trees were soaked in distilled water for 2h before staining. After imbibition, sections were stained in 10 % phloroglucinol-HCl (Jensen 1962) for 1 h, in 0.05 % toluidine blue O (O'Brien et al. 1964) for 15 min, or in Mäule reagent for 10 min (Soukup 2019). Unstained imbibed sections were observed under UV light - excited (358 nm) autofluorescence (Vazquez-Cooz and Meyer 2004). All sections prepared for histochemical analysis were mounted in water, examined, and photographed by a Zeiss Axiovert light-fluorescence microscope (Carl Zeiss GmbH, Göttingen, Germany).

2.3 Scanning electron microscopy (SEM)

Cross sections of dried stems, 100 um thick, were sputtercoated with a thin layer of gold and examined using a TES-CAN VEGA 5130MM scanning electron microscope (SEM, TESCAN, Brno, Czech Republic) in secondary electron imaging mode at an accelerating voltage of 20 kV.

2.4 Raman microspectroscopy

Raman microspectroscopy spectra were recorded using XploRA Raman spectrometer (Horiba Jobin Yvon, Palaiseau, France) equipped with microscope Olympus BX51 (Tokyo, Japan), 50 LWD objective (Olympus, Tokyo, Japan). Raman spectra for fiber c.w.s were recorded using a laser at a wavelength of 532 nm equipped with a 1,200 lines mm⁻¹ grating; spectra were acquired by applying exposure time 10 s and scanning 9–10 cells per sample, using 10 % filter. In NW samples of control P. x euramericana trees Raman spectra were recorded for CML at cell corners and for SCW at the mid region (which corresponds to S₂ as the thickest layer of the SCW). In TFW of bent trees, Raman spectra were recorded for CML at cell corners and for the G-layer at the mid region of the G-layer as the thickest c.w. layer. The spectral resolution was about 3 cm⁻¹ and autocalibration was done each time before recording of spectra by 520.47 cm⁻¹ line of silicon.

2.4.1 Spectroscopic data pre-processing and analysis

The Origin Pro 2018 software was used to preprocess the Raman spectra, including baseline correction, Savitzky-Golay smoothing (10 data points, second-order polynomial), and normalization via Standard Normal Variate (SNV).

3 Results and discussion

3.1 Histochemical and ultrastructural analysis of P. x euramericana NW and TFW

Autofluorescence and different staining methods were used to determine lignin distribution in different c.w. layers of P. x euramericana fibers (Figure 1).

NW fibers exhibit high UV excited autofluorescence intensity (Figure 1A and B), intense violet-red coloration after the phloroglucinol staining (Figure 1D and E), orange coloration after Mäule staining (Figure 1H and I), and dark blue coloration after the toluidine blue O staining (Figure 1L and

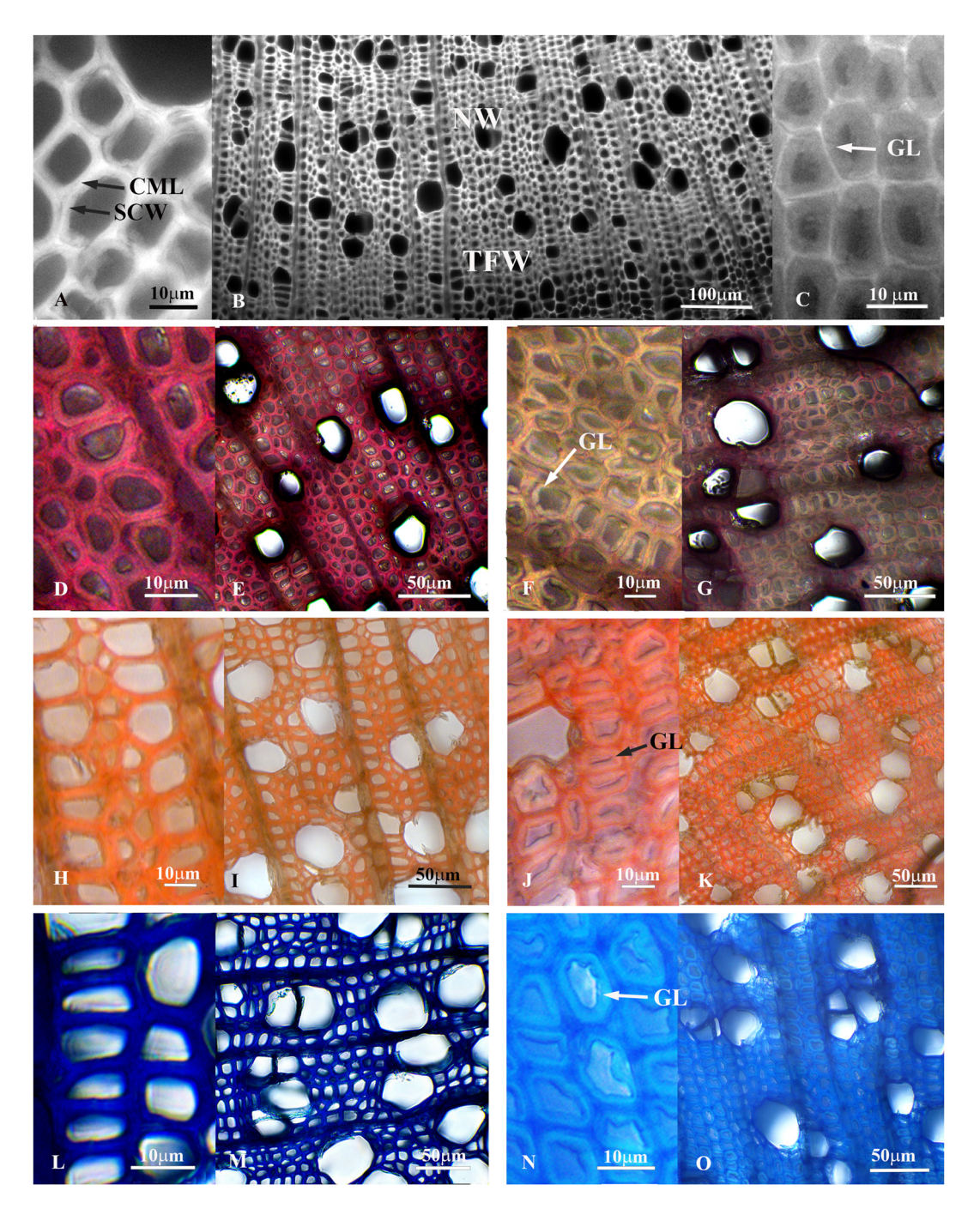


Figure 1: Populus x euramericana cl. NS 11-8 stem cross sections of control and bent trees. (A, B, D, E, H, I, L, M) NW of control trees; (B, C, F, G, J, K, N, O) TFW of bent trees; (B) last two growth rings from bent trees showing the difference in autofluorescence intensity between NW formed before bending treatment was performed, and TFW formed in response to the bending treatment. (A, B, C) UV-excited autofluorescence; (D, E, F, G) phloroglucinol staining; (H, I, J, K) Mäule staining; (L, M, N, O) toluidine blue O staining. NW, normal wood; TFW, tensile flexure wood; CML, compound middle lamellae; SCW, secondary cell wall; GL, gelatinous layer.

M), across the entire c.w., indicating the presence of lignin in all c.w. layers. CML, particularly at cell corners, shows to some extent higher autofluorescence intensity (Figure 1A and B), darker violet-red after the phloroglucinol staining (Figure 1D and E), intense orange coloration after Mäule

staining (Figure 1H and I), and darker blue color after the toluidine blue O staining (Figure 1L and M), suggesting higher lignin content in CML compared to SCW. The highest lignin content, guaiacyl-rich and highly condensed, in CML of NW fibers, particularly at cell corners, compared to inner c.w. layers was demonstrated by various methods, from the Klason and acetyl bromide method to Raman scattering microscopy in fibers of divergent origins (Meshitsuka and Nakano 1985; Zeng et al. 2017; Zhang et al. 2022). In addition, Mäule staining reveals a higher syringyl/guaiacyl (S/G) ratio in P. x euramericana NW fibers (colored orange) compared to the ray parenchyma and vessels (colored brown) (Figure 1H and I). The difference in lignin composition between vessel and fiber cell walls was established in Populus deltoides using confocal fluorescence microscopy: G-rich lignin characterizes vessel cell walls (both CML and SCW), whereas a mixture of S and G lignin characterizes the fiber walls (Donaldson 2013).

In addition, Mäule staining reveals a higher S/G ratio in TFW (colored red-orange, Figure 1]) compared to NW (colored orange, Figure 1H).

In poplar TW fibers the G-layer replaces the S₃ and a part of the S2 layer (Ghislain and Clair 2017; Wardrop and Dadswell 1955), while in TFW fibers, a decrease in S-layer thickness compared to TW is shown (Roignant et al. 2018). Consequently, in P. x euramericana TFW fibers, CML and the thin S-layer on micrographs are visible as one highly lignified c.w. layer (Figure 1B, C, F, G, J, K, N and O), rich in G units (high UV excited autofluorescence intensity, violet-red coloration after phloroglucinol staining, red-orange coloration after Mäule staining, Figure 1B, C, F, G, J and K). In contrast, the G-layer shows weak UV excited autofluorescence (Figure 1C) and almost no coloration after phloroglucinol staining (Figure 1F), indicating that the G-layer contains little to no G lignin. At the same time, weak UV excited autofluorescence (Figure 1C) of the G-layer may represent the presence of S lignin. Fluorescence spectra of G-fibers in P. deltoides showed G-rich lignin in the S2 layer and S-rich lignin at the inner margin of the G-layer (Donaldson 2013). The presence of the S lignin in the G-layer is also indicated by the pale pink coloration after Mäule staining (Figure 1] and K). The light blue coloration after toluidine blue O staining (Figure 1N and O) indicates the presence of phenolic or lignin like substances in the G-layer, whereas the dark blue coloration of the thin border on the lumen surface (Figure 1N) indicates the difference in lignin/phenolic composition compared to the integral G-layer. The dark blue to light blue coloration (Figure 1L–O) of CML, S, and G-layer, respectively, indicates the differences in lignin/phenol structure/content in these c.w. layers of TFW fibers in P. x euramericana. Bowling and Vaughn (2008) used toluidine blue O to demonstrate the presence of an unlignified G-layer colored purple in the G-fibers of Liquidambar styraciflua L., while the lignified G-layer of sclerenchyma cells in the woody stem of monocotyledonous liana Dioscorea balcanica Košanin showed a light blue coloration (Simonović Radosavljević et al. 2017).

Roussel and Clair (2015) showed that the G-layer either has high cellulose content and no lignin or is lignified later during the maturation process in some species. The presence of lignin or lignin-like substances in the G-layer or on its lumen surface has been demonstrated in different tree species (mainly diverse hybrid poplars) using complex techniques. Using transmission electron microscopy, Joseleau et al. (2004) demonstrated that in P. deltoides S lignin units are abundant in the G-layer. Raman microspectrometry (Gierlinger and Schwanninger 2006) in Populus nigra x Populus deltoids showed the presence of small amounts of lignin within the G-layer, but its increase toward the lumen surface. Label-free in situ confocal Raman microscopy in P. nigra (Ma et al. 2013) revealed the presence of a lignin related band at 1.603 cm⁻¹ in the G-layer, though not in high enough concentration to be visualized by the imaging approach. Fluorescence spectroscopy (Donaldson 2013) suggested the presence of syringyl p-hydroxybenzoate-rich lignins at the inner margin of the G-layer of P. deltoides, while Zhao et al. (2021) revealed a unique adaptive mechanism of poplar species to the mechanical stress/gravistimulation, which includes S-lignin-bound p-hydroxybenzoate accumulation in TFW/TW.

SEM micrographs (Figure 2) reveal the differences in the ultrastructure between P. x euramericana NW (Figure 2A-C) and TFW (Figure 2B-D) fibers.

NW fibers show relatively thin cell walls with slightly distinguishable CML and SCW (Figure 2A–C).

In TFW fibers, the G-layer loosened from the S-layer is visible, while CML and the thin S-layer are visible as one layer. The cracks within the G-layer (Figure 2D) and the differences in cellulose microfibrils orientation between the S-layer of NW and G-layer of TFW are observable (Figure 2C and D). These features, the weak adhesion of the G-layer to the preceding S-layer and the cracks within the G-layer, are considered the main features of G-fibers in TW (Clair et al. 2005). The main differences in the orientation of cellulose microfibrils in different c.w. layers can be observed using scanning electron microscopy (SEM), including both conventional and field-emission types, as demonstrated by Simonović Radosavljević et al. (2017) and Ruelle et al. (2007).

3.2 Raman microspectroscopy of P. x euramericana NW and TFW

Raman microspectroscopy analysis focused on direct measurements of fiber's cell walls on P. x euramericana stem cross sections (Figure 3). The CML was measured at the cell corners in both NW fibers of control trees and TFW fibers of bent trees. Although thin c.w. layers (like CML) can be

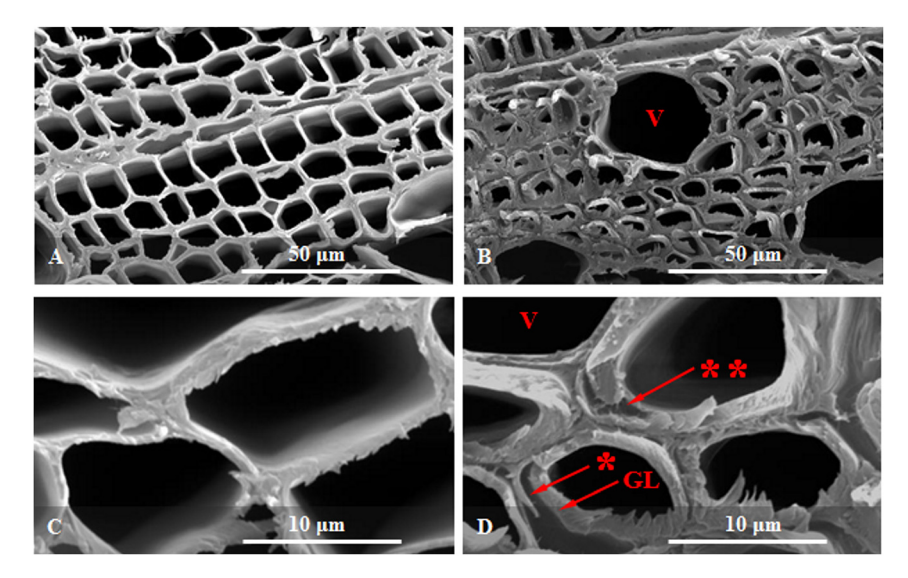


Figure 2: SEM micrographs of *Populus x* euramericana cl. NS 11-8 stem cross sections of control and bent trees: (A. C) normal wood of control trees, and (B, D) tensile flexure wood of bent trees. NW, normal wood; TFW, tensile flexure wood; GL, gelatinous layer; *, detachment of the thick GL from the thin S2 layer of secondary cell wall; **, cracks within the GL due to the shrinkage of the GL; V,

distinguished using Raman microspectroscopy, spectral contributions from the neighboring c.w. layers may overlap (Gierlinger and Schwanninger 2006). In NW fibers, SCW was examined at the mid-region, corresponding to the S₂ layer (SL). In TFW fibers, the G-layer (GL) was measured at the mid-region (Figures 1 and 2).

Figure 3 presents overlaid averaged Raman spectra for the 500–1,800 cm⁻¹ region, derived from 9 to 10 fiber cell walls per sample of NW (CML and SL) and TFW (CML and GL).

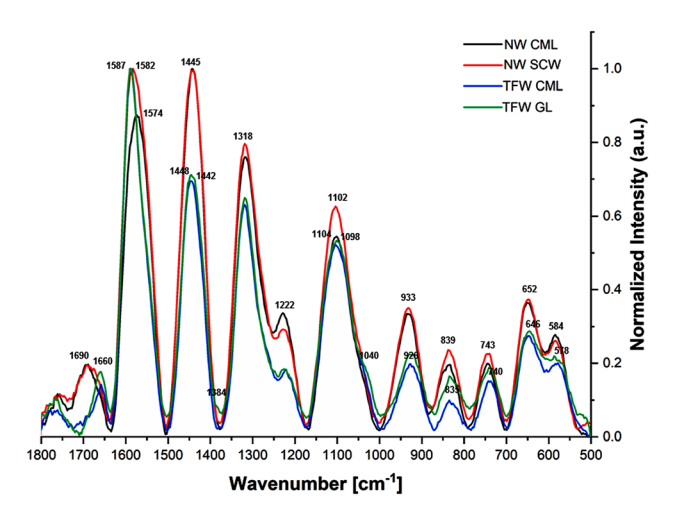


Figure 3: Averaged Raman spectra of Populus x euramericana NW and TFW fiber cell walls recorded in the spectral range from 500 to 1,800 cm⁻¹. NW CML, compound middle lamella of normal wood fibers (measured at cell corners); NW SL, secondary cell wall of normal wood fibers (measured at the mid region, corresponding to the S₂ layer, as the thickest layer of the SCW in NW fibers); TFW CML, compound middle lamella of tensile flexure wood fibers (measured at cell corners); TFW GL, gelatinous layer of tensile flexure wood fibers (measured at the mid region). Assignments of the bands characteristic of c.w. polymers and the corresponding references for assignation are provided in Table 1.

Table 1 provides the assignments of the bands characteristic for c.w. polymers and the corresponding references for assignation.

The region between 1,200 and 1,700 cm⁻¹ reflects the spectral contribution of lignin or lignin-like compounds. The 600-1,100 cm⁻¹ region is dominated by cellulose, hemicellulose, and pectin.

Small changes in band positions and intensities can provide insights into alterations in polymer composition and orientation. Several factors, including the amount, composition, orientation, crystallinity, and linkages to other components, contribute to the spectral changes (Gierlinger and Burgert 2006). Shifts in peak position arise from variations in the length of chemical bonds or the positions of the atoms. Shifts to lower wavenumbers result from longer bond length (and tensile strain), and vice versa shifts to higher wavenumbers suggest shorter bond length (compressive strain, higher strength) (Tuschel 2019). On the other hand, variations in band width reflect the uniformity of bond lengths; narrowing band widths suggests structural arrangement or order - the weaker the chemical interaction, the narrower the band will be (Tuschel 2019).

The region around 1,600 cm⁻¹ contains the main marker band of lignin assigned to symmetric aromatic ring stretching vibrations (Table 1). It informs on lignin structure and ring orientation or the lignin microenvironment, the alignment of S and G units, and it deffers in different wood species (Larsen and Barsberg 2010). In this region, two bands characterize P. x euramericana NW, 1,574 cm⁻¹ (CML) and 1,582 cm⁻¹ (S-layer), suggesting the difference in lignin structure; a shorter bond length and higher strength of lignin structure characterize the S-layer compared to the CML. In TFW, shift to the higher wavenumber (1,587 cm⁻¹) compared to NW is visible in both

Table 1: Assignment of the Raman bands characteristic for the polymers in the cell walls of *Populus x euramericana*, and the corresponding references used for assignation.

Wavenumber (cm ⁻¹)	Vibrational mode	Chemical moiety	Reference sources
1,690, 1,660	C=C in coniferyl alcohol or C=O in coniferyl aldehyde	Lignin	Agarwal (2006), Agarwal et al. (2011), Gao et al. (2021), Zhang (2021) and Zhu et al. (2018)
~1,585, 1,574	Symmetric aro- matic ring stretch- ing vibrations	Lignin	Agarwal (2006), Agarwal et al. (2011), Gao et al. (2021), Gierlinger et al. (2008)
~1,455, 1,442	O–CH ₃ deformation; CH ₂ scissoring; guaiacyl/syringyl ring	Lignin	Agarwal et al. (2011), Agarwal (2019), Gierlinger and Schwanninger (2006), and Larsen and Barsberg (2010)
1,384	C-O-C stretching	Cellulose	Agarwal (2019) and Gierlinger et al. (2012)
1,318	Aromatic ethers stretching	S Unit	Agarwal and Atalla (2010)
1,306	G ring mode with C=O group	Coniferyl alcohol	Agarwal et al. (2011) and Gao et al. (2021)
~1,222	Aryl-O of aryl-OH and aryl-O-CH ₃ ; guaiacyl/syringyl ring (with C=O	G ring mode of lignin	Agarwal et al. (2011) and Gier- linger et al. (2008)
1,098–1,104	group) mode Glycosidic C–O–C asymmetric and symmetric stretching vibrations	Cellulose or hemicellulose	Agarwal (2006), Gao et al. (2021), Gierlinger et al. (2008), Gierlinger and Schwanninger (2007), Szymańska- Chargot et al. (2015), and Zhang (2021)
1,036	C–O of aryl O–CH ₃ and aryl OH, C–O stretching vibration	Cellulose	Agarwal et al. (2011), Gao et al. (2021), Gierlinger et al. (2008), and
1,040	OC stretching; ring deformation, CH ₃ wagging	Lignin	Gierlinger and Schwanninger (2006)
939–925	C-C-H waging vibration, C-O-H bending vibration	Lignin	Agarwal et al. (2011) and Synytsya et al. (2003)
848-833	C-O-C skeletal modes	Pectin, hemicellulose	Agarwal (2014) and Synytsya et al. (2003)

Table 1: (continued)

Wavenumber (cm ⁻¹)	Vibrational mode	Chemical moiety	Reference sources
750–736	Skeletal deformation	Lignin	Agarwal et al. (2011)
658-652, 635	C–O–C skeletal modes	Pectin	Szymańska- Chargot et al. (2015)
584–578	Skeletal deformation	Lignin	Agarwal (2014) and Agarwal et al. (2011)

CML and GL (Figure 3, Table 1). However, the narrowing of the band at 1,587 cm⁻¹ characterizing TFW, despite its shift to a higher wavenumber, suggests weaker chemical interactions relative to the shift.

The main marker band of lignin is accompanied by the band at 1,657 cm⁻¹ assigned to coniferyl alcohol or coniferyl aldehyde, precursors of lignin. In hardwood lignin, this band may exhibit different contributions from sinapyl alcohol and sinapaldehyde units. In *Populus euramericana* TFW this band shifts to the lower wavenumber (1,660 cm⁻¹) and became narrower compared to NW (1,690 cm⁻¹), suggesting tensile strain, and weaker chemical interactions.

As opposed to *P. euramericana* TFW (Figure 3), in grounded samples of TW of the inclined stem of *P. euramericana* Raman spectroscopy (Guan et al. 2021) showed no shift in the main marker band of lignin, assigned to symmetric aromatic ring stretching vibrations, while the band assigned to coniferyl alcohol and coniferyl aldehyde shifted to the lower wavenumber in TW compared to NW. In contrast, in TW of the inclined stem of *P. nigra* label-free *in situ* Raman microspectroscopy revealed no shifts in band positions in the region 1,700–1,500 cm⁻¹ region compared to OW (Ma et al. 2013).

The high intensity band assigned to guaiacyl/syringyl ring vibration (1,445 cm $^{-1}$) decreased considerably in *P. euramericana* TFW compared to NW (Figure 3, Table 1), while in the spectra of the G-layer, a doublet at 1,448 cm $^{-1}$ and 1,442 cm $^{-1}$ is visible.

A shoulder at 1,384 cm⁻¹, a non-orientation-sensitive cellulose band (Agarwal 2019; Gierlinger et al. 2012), is visible only in the G-layer of TFW.

The bands at 1,222 and 1,318 cm⁻¹, characteristic of G and S lignin units, respectively, indicate the higher content of S compared to G unit in both NW and TFW, and suggest the higher S/G ratio in TFW compared to NW fibers (Figure 3, Table 1), already indicated by Mäule staining (Figure 1H–K). Similarly to TFW (Figure 3, Table 1), lower lignin content and higher S/G ratio were shown in TW of *P. euramericana* compared to NW (Guan et al. 2021).

he bands in the region from 1,090 to 1,120 cm⁻¹, characteristic for glycosidic C-O-C asymmetric and symmetric stretching vibrations in cellulose or hemicellulose, mainly xyloglucan and glucomannan, represent the most orientationsensitive cellulose band. This broad band includes both carbohydrate concentration and orientation changes (Gierlinger and Schwanninger 2006). Consequently, changes in the amount cannot be accurately investigated by the band integration, as they include changes in cellulose microfibril orientation and/or crystallinity (Gierlinger 2017). A strong correlation between the shift of this band and the applied strain was found (Gierlinger 2017); with the increasing strain, this band shifted remarkably to lower wavenumbers (Gierlinger et al. 2006). Ma et al. (2013) showed that in P. nigra, this band in the OW fiber S2 layer (at 1.097 cm⁻¹) shifted to lower wavenumbers in the TW fibers. both S₂ layer (1,094.4 cm⁻¹) and G-layer (1,094 cm⁻¹), meaning that both S2 and G-layer respond to leaning by the changes of the same direction in cellulose microfibril orientation (tensional deformations of the glycosidic C-O-C bond of cellulose).

In juvenile P. x euramericana (Figure 3, Table 1), this band at 1,102 cm⁻¹ in NW fibers (both CML and S-layer) shifted to a lower wavenumber (1,098 cm⁻¹) in the G-layer of TFW, suggesting tensional deformations. However, in the CML of TFW (it should be noted that in thin c.w. layers, the spectral contributions from the neighboring c.w. layers may overlap; Gierlinger and Schwanninger 2006), this band shifted to a higher wavenumber (1,104 cm⁻¹), suggesting a shorter bond length and compressive strain (higher strength) in the glycosidic C-O-C bond of cellulose. In other words, CML and G-layer of P. euramericana TFW fibers respond to long-term severe static bending by opposite changes in cellulose microfibril orientation; compressive strain (higher strength) characterizes the glycosidic C-O-C bond of cellulose in CML, opposed to tensile strain (weaker chemical interactions) in the G-layer.

A shoulder at 1,040 cm⁻¹, visible only in the G-layer of TFW (Figure 3, Table 1), is suggested to be linked to lignin (Gao et al. 2021; Gierlinger and Schwanninger 2006).

The band at 939 cm⁻¹, characteristic of C-C-H waging vibration, or C-O-H bending vibration in lignin (Figure 3, Table 1), shifted to lower wavenumbers (926 cm⁻¹) in TFW. Also, bands at 750-736 cm⁻¹ and 584-578 cm⁻¹, characteristic of skeletal deformations in lignin, shifted to lower wavenumbers in TFW compared to NW (Figure 3, Table 1).

The bands at around 835 and 655 cm⁻¹ characteristic for pectin (Table 1) are the most prominent Raman markers for pectin polysaccharides, without overlapping with other c.w. polymers. The wavenumber positions of these bands are shifted for pectin with a different degree of methylesterification (Synytsya et al. 2003; Szymańska-Chargot et al. 2015; Zhu et al. 2018). The band at 839 cm $^{-1}$ in P. x euramericana NW fibers shifted to lower wavenumbers (835 cm⁻¹) in TFW (Figure 3), while the band at 652 cm⁻¹ in NW fibers shifted to 646 cm⁻¹ in TFW. These shifts suggest the differences in pectin methylesterification (Synytsya et al. 2003; Szymańska-Chargot et al. 2015; Zhu et al. 2018) in TFW compared to NW (Figure 3).

3.3 The difference in cell wall structure of TFW (Figures 1, 2, and 3) and TW (literature data)

The difference in c.w. structure of TFW fibers compared to TW fibers, a thinner G-layer (with a higher microfibrillar angle), and a thinner S-layer (Niez et al. 2020; Roignant et al. 2018), are determined by structural differences of c.w. polymers. Heinrich and Gärtner (2008), Robards (1966) and Wilson and Gartner (1996) suggested that the tension wood severity in angiosperms, similar to compression wood severity in gymnosperms, is related to the degree of lean from the vertical or to the severity of bending treatments. However, Urbancsok et al. (2023) showed that the transcriptional program of TFW only partially overlapped the TW program.

Comparison of c.w. structural differences between TW formed in the inclined stem of P. euramericana (Raman spectroscopy, Guan et al. 2021) and P. nigra (label-free in situ Raman microspectroscopy, Ma et al. 2013) with presented Raman microspectroscopy results on TFW of P. euramericana (Figure 3) formed as a response to long term static bending treatment, suggest significant difference in c.w. structure between TW and TFW.

In TW of P. euramericana (grounded samples, Guan et al. 2021) and P. nigra (S2 and G-layer, Ma et al. 2013), the difference in the structure of c.w. polymers was only visible in the shifts to the lower wavenumbers of the bands assigned to coniferyl alcohol and coniferyl aldehyde (compared to NW, Guan et al. 2021) and bands assigned to glycosidic C-O-C stretching vibrations, the most orientation-sensitive cellulose band (compared to OW, Ma et al. 2013).

In contrast, in TFW of P. euramericana (Figure 3, Table 1), differences in the structure of lignin, cellulose, hemicellulose, and pectin are suggested compared to NW.

The difference in the structure of lignin in TFW compared to NW is suggested based on the shifts of the bands: at 1,587 with the dominant spectral contribution of lignin, at 1,687 cm⁻¹ characteristic for coniferyl alcohol or coniferaldehyde, at 933, 750, and 584 cm⁻¹ characteristic for waging vibrations and skeletal deformations of lignin, as well as the shoulder at 1,040 cm⁻¹ visible only in G-layer.

The difference in the structure of cellulose and hemicellulose in TFW compared to NW is suggested based on the shifts of the bands at around 1,100 cm⁻¹ (the most orientation-sensitive cellulose band), and the shoulder at 1,384 cm⁻¹ visible only in G-layer (a non-orientation-sensitive cellulose band).

The difference in methyl esterification of pectin in TFW compared to NW is suggested by the shifts of the bands at 839 and 652 cm⁻¹.

In this regard, a comprehensive and detailed study of TW formation as a response to precisely controlled leaning treatments, as well as TFW formation as a response to precisely controlled bending treatments, would be of great importance for understanding the similarities and differences in the structure of c.w. polymers between TW and TFW.

3.4 TFW as an increased source of nonrecalcitrant cellulose for biofuel production

Urbancsok et al. (2023) showed that low-intensity stem flexing stimulates growth, while induced TFW, similarly to TW (Donaldson and Singh 2016), represents an increased source of non-recalcitrant cellulose for biofuel production. The efficiency of bioethanol production depends on lignocellulose composition. It increases with higher cellulose content (Serapiglia. et al. 2013), lower cellulose crystallinity (hemicellulose/cellulose ratio) (Li et al. 2014), pectin acetylation levels (Xiao and Anderson 2013), lower lignin content (Li et al. 2014; Serapiglia, et al. 2013), higher syringyl (S) to guaiacyl (G) ratio (Kang et al. 2014), higher coniferaldehyde content (Yamamoto et al. 2020), and lower ash content (Kang et al. 2014).

Presented preliminary data suggest the difference in the structure of lignin, coniferyl alcohol and coniferaldehyde, cellulose, hemicellulose, and pectin methyl esterification, as well as the higher S/G ratio in TFW compared to NW (Figures 1 and 3). These findings encourage further investigation on P. euramericana TFW for biofuel production. Planting P. euramericana, a fast-growing tree species, as windbreak forests to block the prevailing winds could provide TFW as an increased source of non-recalcitrant cellulose for biofuel production.

4 Conclusions

The presence of lignin in the G-layer, higher S/G ratio, as well as the differences in lignin structure in different c.w. layers

between TFW and NW fibers in P. x euramericana, indicated by histochemical analysis, was confirmed by Raman microspectroscopy. Additionally, Raman microspectroscopy suggested the difference in cellulose and hemicellulose structure and pectin methylesterification in TFW compared to NW. The G-layer and CML contribute to the response to long-term severe static bending by opposite shifts of the band attributed to the glycosidic C-O-C bond, the most orientation sensitive cellulose band, suggesting opposite changes in cellulose microfibril orientation; higher strength characterizes cellulose in CML, opposed to weaker chemical interactions in the G-layer.

SEM showed the c.w. ultrastructure of TFW fibers: G-layer loosened from the thin S-layer, cracks within the G-layer, and the differences in cellulose microfibrils orientation/arrangement compared to S-layer of NW.

These preliminary data encourage further investigation of TFW, focusing on both changes in c.w. structure as a mechanical acclimation to stem bending and its potential for biofuel production.

Acknowledgments: The authors wish to thank the Institute of Lowland Forestry and Environment, University of Novi Sad, for providing Populus x euramericana cl. NS 11-8 cuttings.

Research ethics: Not applicable. **Informed consent:** Not applicable.

Author contributions: A.Lj.M.: designed the research; D.J., A.Lj.M.: histochemical analysis; K.V.: SEM; I.P.: Raman microspectroscopy. I.P., D.B., A.Lj.M.: Raman data analysis and results interpretation. A.Lj.M.: wrote the paper with input from all authors. All authors read and approved the manuscript.

Use of Large Language Models, AI and Machine Learning **Tools:** None declared.

Conflict of interest: The authors declare that they have no conflicts of interest regarding this article.

Research funding: This work was supported by the Ministry of Education, Science and Technological Development of the Republic of Serbia (contract nos. 451-03-136/2025-03/200053, 451-03-137/2025-03/200178, 451-03-137/2025-03/200116).

Data availability: Not applicable.

References

Abedini, R., Clair, B., Pourtahmasi, K., Laurans, F., and Arnould, O. (2015). Cell wall thickening in developing tension wood of artificially bent poplar trees. IAWA J 36: 44-57.

Agarwal, U.O., McSweeny, J.D., and Ralph, S.A. (2011). FT-Raman investigation of milled-wood lignins: softwood, hardwood, and chemically modified black spruce lignins. JWCT 31: 324-344.

- Agarwal, U.P. (2006). Raman imaging to investigate ultrastructure and composition of plant cell walls: distribution of lignin and cellulose in black spruce wood (Picea mariana). Planta 224: 1141-1153.
- Agarwal, U.P. (2014). 1064 nm FT-Raman spectroscopy for investigations of plant cell walls and other biomass materials. Front. Plant Sci. 5: 490.
- Agarwal, U.P. (2019). Analysis of cellulose and lignocellulose materials by Raman spectroscopy: a review of the current status. *Molecules* 24:
- Agarwal, U.P. and Atalla, R. (2010). Vibrational spectroscopy. In: Heitner, C., Dimmel, D.R., and Schmidt, J.A. (Eds.). Lignin and lignans advances in chemistry. CRC Press, Boca Raton, FL, chapter 4, pp. 103-136.
- Bowling, A.J. and Vaughn, K.C. (2008). Immunocytochemical characterization of tension wood: gelatinous fibers contain more than just cellulose. Am. J. Bot. 95: 655-663.
- Clair, B., Thibaut, B., and Sugiyama, J. (2005). On the detachment of gelatinous layer in tension wood fibre. JWCT 51: 218-221.
- Dadswell, H.E. and Wardrop, A.B. (1955). The structure and properties of tension wood. Holzforschung 9: 97-104.
- Donaldson, L.A. (2013). Softwood and hardwood lignin fluorescence spectra of wood cell walls in different mounting media. IAWA J 34: 3-19.
- Donaldson, L.A. and Singh, A.P. (2016). Reaction wood. In: Kim, Y.S. (Ed.). Secondary xylem biology. Elsevier, Amsterdam, pp. 93-110.
- Gao, W., Shu, T., Liu, Q., Ling, S., Guan, Y., Liu, S., and Zhou, L. (2021). Predictive modeling of lignin content for the screening of suitable poplar genotypes based on Fourier transform-Raman spectrometry. ACS Omega 6: 8578-8587.
- Ghislain, B. and Clair, B. (2017). Diversity in the organisation and lignification of tension wood fibre walls: a review. IAWA J. 38: 245-265.
- Gierlinger, N. (2017). New insights into plant cell walls by vibrational microspectroscopy. Appl. Spectrosc. Rev. 53: 517-551.
- Gierlinger, N. and Burgert, I. (2006). Secondary cell wall polymers studied by confocal Raman microscopy: spatial distribution, orientation, and molecular deformation. N. Z. J. For. Sci. 36: 60-71.
- Gierlinger, N. and Schwanninger, M. (2006). Chemical imaging of poplar wood cell walls by confocal Raman microscopy. Plant Physiol. 140:
- Gierlinger, N., Schwanninger, M., Reinecke, A., and Burgert, I. (2006). Molecular changes during tensile deformation of single wood fibers followed by Raman microscopy. Biomacromolecules 7: 2077-2081.
- Gierlinger, N. and Schwanninger, M. (2007). The potential of Raman microscopy and Raman imaging in plant research. Spectroscopy 21:
- Gierlinger, N., Goswami, L., Schmidt, M., Burgert, I., Coutand, C., Rogge, T., and Schwanninger, M. (2008). In situ FT-IR microscopic study on enzymatic treatment of poplar wood cross-sections. Biomacromolecules 9: 2194-2201.
- Gierlinger, N., Keplinger, T., and Harrington, M. (2012). Imaging of plant cell walls by confocal Raman microscopy. Nat. Protoc. 7: 1694-1708.
- Guan, Y., Shua, T., Gao, H., Zhou, L., and Zhang, L. (2021). Comparative studies on lignin structures in normal and tension wood of *Populus* × euramericana cv. "74/76". Int. J. Biol. Macromol. 172: 178-185.
- Heinrich, I. and Gärtner, H. (2008). Variations in tension wood of two broadleaved tree species in response to different mechanical treatments: implications for dendrochronology and mass movement studies. IJPS
- Jensen, W.A. (1962). *Botanical histochemistry: principles and practice*. W.H. Freeman and Company, San Francisco, California.
- Joseleau, J.P., Imai, T., Kuroda, K., and Ruel, K. (2004). Detection in situ and characterization of lignin in the G-layer of tension wood fibers of Populus deltoides. Planta 219: 338-345.

- Kang, Q., Appels, L., Tan, T., and Dewil, R. (2014). Bioethanol from lignocellulosic biomass: current findings determine research priorities. Sci. World J.: 298153, https://doi.org/10.1155/2014/298153.
- Larsen, K.L. and Barsberg, S. (2010). Theoretical and Raman spectroscopic studies of phenolic lignin model monomers. J. Phys. Chem. B 114: 8009-8021.
- Li, L., Zhou, W., Wu, H., Yu, Y., Liu, F., and Zhu, D. (2014). Relationship between crystallinity index and enzymatic hydrolysis performance of celluloses separated from aquatic and terrestrial plant materials. BioResources 9: 3993-4005.
- Ma, J., Zhou, X., Zhang, X., and Xu, F. (2013). Label-free in situ Raman analysis of opposite and tension wood in Populus nigra. BioResources 8:
- Meshitsuka, G. and Nakano, J. (1985). Structural characteristics of compound middle lamella lignin. I. Wood Chem. Technol. 5: 391–404.
- Niez, B., Dlouha, J., Gril, J., Ruelle, J., Toussaint, E., Moulia, B., and Bade, E. (2020). Mechanical properties of "flexure wood": compressive stresses in living trees improve the mechanical resilience of wood and its resistance to damage. Ann. For. Sci. 77: 17.
- O'Brien, T.P., Feder, N., and McCully, M.E. (1964). Polychromatic staining of plant cell walls by toluidine blue O. Protoplasma 59: 368-373.
- Prokopijević, M., Simonović Radosavljević, J., Spasojević, D., Vojisavljević, K., Radotić, K., and Mitrović, A.L. (2022). XET activity determination in powdered wood samples as an indicator of tension wood, tested on juvenile Populus x euramericana exposed to severe long-term static bending. Holzforschung 76: 668-673.
- Robards, A.W. (1966). The application of the modified sine rule to tension wood production and eccentric growth in the stem of crack willow (Salix fragilis L.). Ann. Bot. 30: 513-523.
- Roignant, J., Badel, É., Leblanc-Fournier, N., Brunel-Michac, N., Ruelle, J., Moulia, B., and Decourteix, M. (2018). Feeling stretched or compressed? The multiple mechanosensitive responses of wood formation to bending. Ann. Bot. 121: 1151-1161.
- Roussel, J.R. and Clair, B. (2015). Evidence of the late lignification of the G-layer in simarouba tension wood, to assist understanding how non-G-layer species produce tensile stress. Tree Physiol. 35: 1366–1377.
- Ruelle, J., Yamamoto, H., and Thibaut, B. (2007). Growth stress and cellulose structural parameters in tension and normal wood from three tropical rainforest angiosperm species. BioResources 2: 235-251.
- Scurfield, G. (1973). Reaction wood: its structure and function: lignification may generate the force active in restoring the trunks of leaning trees to the vertical. Science 179: 647-655.
- Serapiglia, M.J., Humiston, M.C., Xu, H., Hogsett, D., de Orduña, R.M., Stipanovic, A.J., and Smart, L.B. (2013). Enzymatic saccharification of shrub willow genotypes with differing biomass composition for biofuel production. Front. Plant Sci. 4: 57.
- Simonović Radosavljević, J., Bogdanović Pristov, J., Mitrović, A.Lj., Steinbach, G., Mouille, G., Tufegdžić, S., Maksimović, V., Mutavdžić, D., Janošević, D., Vuković, M., et al. (2017). Parenchyma cell wall structure in twining stem of Dioscorea balcanica. Cellulose 24: 4653-4669.
- Soukup, A. (2019). Selected simple methods of plant cell wall histochemistry and staining for light microscopy. Plant cell morphogenesis: methods and protocols. Methods Mol. Biol. 1992: 27-42.
- Synytsya, A., Copikova, J., Matejka, P., and Machovic, V. (2003). Fourier transform Raman and infrared spectroscopy of pectins. Carbohydr. Polym. 54: 97-106.
- Szymańska-Chargot, M., Chylinska, M., Kruk, B., and Zdunek, A. (2015). $Combining \ FT-IR \ spectroscopy \ and \ multivariate \ analysis \ for \ qualitative$ and quantitative analysis of the cell wall composition changes during apples development. Carbohydr. Polym. 115: 93-103.

- Telewski, F.W. (1989). Structure and function of flexure wood in Abies fraseri. Tree Physiol. 5: 113-121.
- Timell, T.E. (1969). The chemical composition of tension wood. Svensk Papperstidning 72: 173–181.
- Tuschel, D. (2019). Raman spectroscopy and polymorphism. Spectroscopy 34: 10-21.
- Urbancsok, I., Donev, E.N., Sivan, P., van Zalen, E., Barbut, F.R., Derba-Maceluch, M., Šimura, J., Yassin, Z., Gandla, M.L., Karady, M., et al. (2023). Flexure wood formation via growth reprogramming in hybrid aspen involves jasmonates and polyamines and transcriptional changes resembling tension wood development. New Phytol. 240: 2312-2334.
- Vazquez-Cooz, I. and Meyer, R.W. (2004). Occurrence and lignification of libriform fibers in normal and tension wood of red and sugar maple. Wood Fiber Sci. 36: 56-70.
- Wardrop, A.B. and Dadswell, H.E. (1955). The nature of reaction wood. IV. Variation in the cell wall organization of tension wood fibres. Aust. J. Bot. 3: 177-189.

- Wilson, B.F. and Gartner, B.L. (1996). Lean in red alder (Alnus rubra): growth stress, tension wood, and righting response. Can. J. For. Res. 26: 1951-1956.
- Xiao, C. and Anderson, C.T. (2013). Roles of pectin in biomass yield and processing for biofuels. Front. Plant Sci. 4: 44594.
- Yamamoto, M., Blaschek, L., Subbotina, E., Kajita, S., and Pesquet, E. (2020). Importance of lignin coniferaldehyde residues for plant properties and sustainable uses. ChemSusChem 13: 4400-4408.
- Zhao, Y., Yu, X.H., and Liu, C.J. (2021). The inducible accumulation of cell wallbound p-hydroxybenzoates is involved in the regulation of gravitropic response of poplar. Front. Plant Sci. 12: 755576.
- Zeng, Y., Himmel, M.E., and Ding, S.Y. (2017). Visualizing chemical functionality in plant cell walls. Biotechnol. Biofuels 10: 263.
- Zhang, X. (2021). Visualising lignin quantitatively in plant cell walls by micro-Raman spectroscopy. *RSC Adv.* 11: 13124–13129.
- Zhang, X., Li, L., and Xu, F. (2022). Chemical characteristics of wood cell wall with an emphasis on ultrastructure: a mini-review. Forests 13: 439.
- Zhu, N., Wu, D., and Chen, K. (2018). Label-free visualization of fruit lignification: Raman molecular imaging of loquat lignifed cells. Plant Methods 14: 58.